Materials Letters 303 (2021) 130585

Contents lists available at ScienceDirect

Materials Letters

journal homepage: www.elsevier.com/locate/matlet

Excellent strength-toughness synergy in metastable austenitic stainless steel due to gradient structure formation

D.O. Panov [a,*], R.S. Chernichenko [a], S.V. Naumov [a], A.S. Pertcev [b], N.D. Stepanov [a], S. V. Zherebtsov [a], G.A. Salishchev [a]

[a] Laboratory of Bulk Nanostructured Materials, Belgorod State University, 85 Pobeda Str., 308015 Belgorod, Russia
[b] Department Chief Metallurgist, Perm Scientific-Research Technological Institute, 41 Geroev Khasana street, 614990 Perm, Russia

ARTICLE INFO

Keywords:
Gradient structure
Metastable austenitic stainless steel
Impact toughness
Strength

ABSTRACT

The effect of cold swaging and subsequent annealing on the structure and mechanical properties of a 321-type metastable austenitic stainless steel was studied. Cold swaging to a strain of 90% produced a gradient structure with a gradual decrease in the α-phase content from the edge to the center of the bar. Globular and lamellar regions of both strain-induced martensite and retained austenite were found in the center, meanwhile, a completely globular austenite–martensite dual-phase structure was formed at the edge. After annealing at 500 °C, (~30° below the reverse martensite-to-austenite phase transformation temperature) microstructure refinement due to simultaneous development of recrystallization and reverse martensite-to-austenite transformation was observed. Both ultimate tensile strength and yield strength increased noticeably after the annealing. Besides, notch toughness of the annealed specimen doubled in comparison to that of the cold-swaged condition and almost reached the level of a coarse-grained condition.

1. Introduction

Metastable austenitic stainless steels (MASS) have a very attractive combination of ductility, impact toughness, and corrosion resistance; at the same time MASS exhibit rather low yield strength [1]. The formation of a gradient structure has been suggested as a promising way to enhance simultaneously the strength and ductility [2,3]. The gradient structure in MASS can be obtained, for example, by torsional deformation [2] or surface mechanical attrition [3]. However, the formation of a bulk gradient structure by swaging is possible due to the uniform plastic deformation [4]. Post-deformation phase reverse annealing might also lead to the heterogeneous structure formation, thereby resulting in an attractive strength-ductility combination [5]. Meanwhile, annealing of cold-deformed MASS at temperatures which is slightly below the lower bound (A_S) of the interval of the reverse martensite-to-austenite phase transformation, might be a promising approach because such annealing can cause additional structure refinement and hardening [6]. Furthermore, partial recovery might also improve strength [7]. It is unclear yet how the low-temperature annealing influences on properties of MASS. The present study intends to reveal the effect of the low-temperature annealing on the structure and mechanical properties of a metastable austenitic stainless steel after cold swaging.

2. Experimental procedures

In the current work, a commercial AISI 321-type steel (wt.%: C-0.07, Cr-18.75, Ni-9.20, Ti-0.59, Mn-1.12, Si-0.39, S-0.005, P-0.019, and Fe-balance) in a form of hot-rolled and water-quenched at 1050 °C bar was used as a starting material. Then, the bar was swaged at room temperature using a SXP-16 forging machine from ∅33.0 to ∅11.5 mm that corresponded to a total strain of 90% [8]. Annealing of the deformed bar was carried out at 500 °C for 2 h. The microstructure was examined by a JEOL JEM-2100 electron microscope in a plain normal to RD. The Vickers hardness was examined along a diameter of the bar using a Wolpert 402MVD semi-automatic hardness tester; a load and dwell time were 200 g and 15 s, respectively. The content of the magnetic α-phase was determined on the previously mechanically ground and polished surface of cross-sections using a FERRITSCOPE FMP30 apparatus which was previously calibrated using standard samples. Tensile tests were conducted on an Instron 5882 electromechanical testing system at a strain rate of $1 \times 10^{-3}s^{-1}$ using specimens with the gage size ∅5mm × 25 mm. The notch toughness was examined using an

* Corresponding author.
E-mail address: panov_d@bsu.edu.ru (D.O. Panov).

https://doi.org/10.1016/j.matlet.2021.130585
Received 31 May 2021; Received in revised form 15 July 2021; Accepted 30 July 2021
Available online 31 July 2021

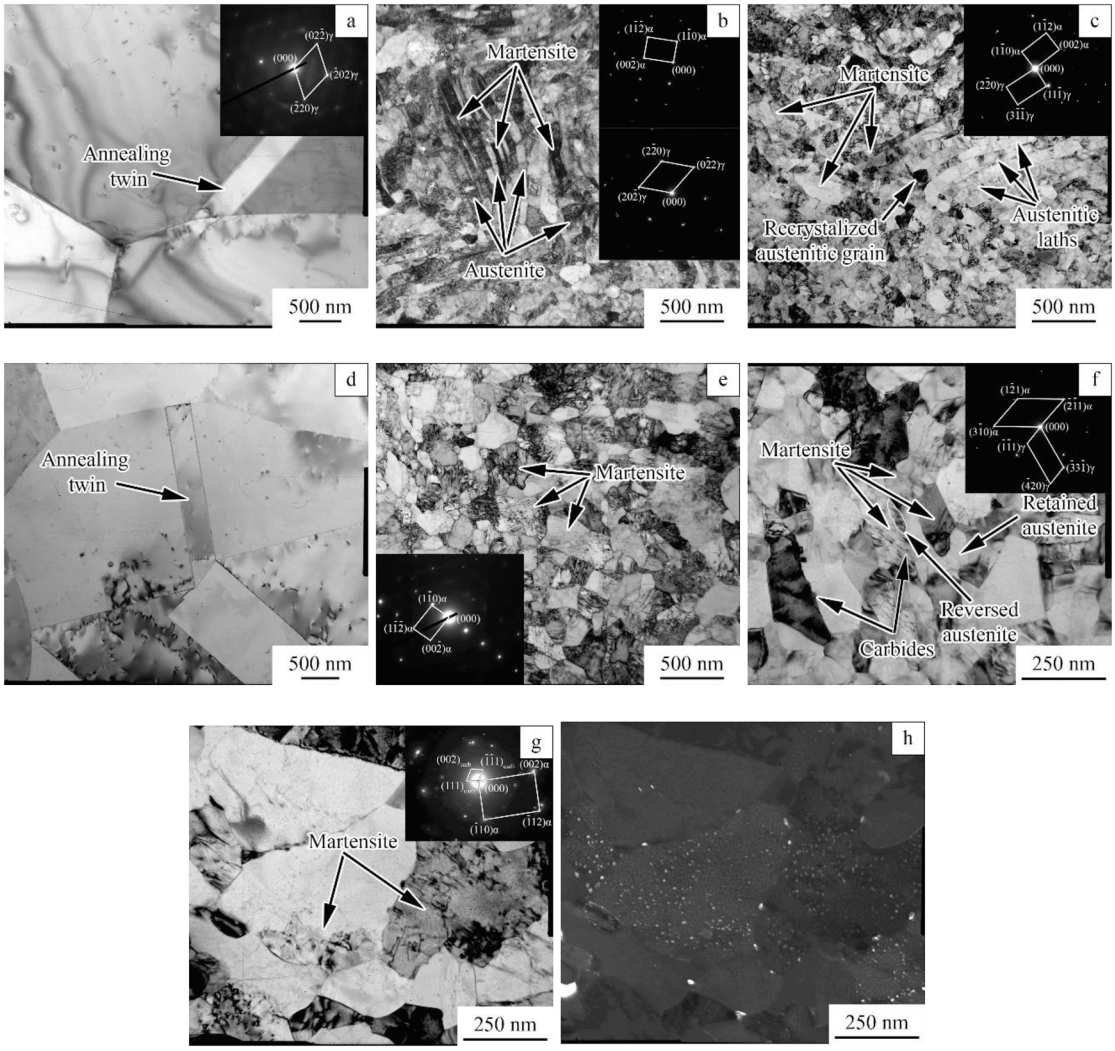

Fig. 1. TEM micrographs of (a), (d) the initial condition; (b), (e) the swaged bar; (c), (f), (g), (h) swaged and annealed at 500 °C condition; (a)–(c) center and (d)–(h) edge of the bar. (h) is dark field in $(22\overline{2})_{carb}$ reflection of a $Me_{23}C_6$-type carbide from (g). Note higher magnification in (f)–(h).

Instron SI-1 M Charpy impact testing machine and pre-cracked specimens (measured 5 × 11 × 55 mm^3). The fatigue crack with a length of ~ 1.5 mm was introduced using a V-shaped notch of ~1.5 mm depth as the crack starter. Specimens for both tensile tests and Charpy impact tests were cut from the central part of the bar along the axial direction. At least two specimens were used for each experimental point. The fracture surface was characterized using a FEI Nova NanoSEM 450 scanning electron microscope. The ratio of the plain strain zone and total fracture surface area was estimated using the SEM-overviews of fracture surfaces. The total fracture surface area was the sum of the plane strain zone and shear lips areas (see Supplementary materials, Fig. S1).

3. Results and discussion

The microstructure of the initial condition consisted of equiaxial austenitic grains ~ 10 μm in diameter; annealing twins, and uniformly

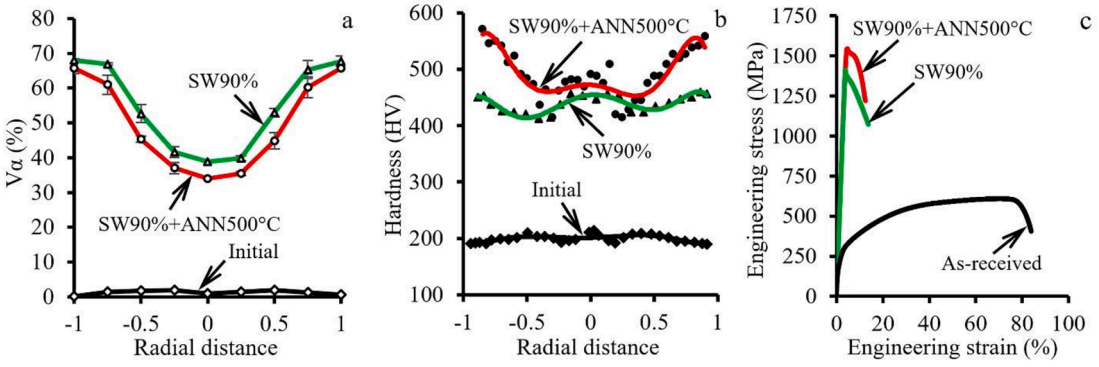

Fig. 2. Distributions of (a) α-phase and (b) microhardness along the section of the bar after different treatment modes; (c) tensile stress–strain curves.

Table 1
Mechanical properties of the 321-type steel.

Condition	YS, MPa	UTS, MPa	δ, %	Notch toughness, MJ/m^2
Initial	155	610	83.2	1.58
Swaging 90%	1405	1410	11.2	0.70
Swaging 90% + annealing 500 °C	1490	1550	9.5	1.42

distributed dislocation were observed in grains (Fig. 1a and d). After swaging, globular and lamellar regions of both strain-induced martensite and retained austenite with a grain/subgrain size of ~ 170 nm were found in the center (Fig. 1b). Hence, the transformation of the lamellar structure into a globular one had not been completed. At the same time, a mainly globular austenite–martensite structure was obtained at the edge after swaging (Fig. 1e). Annealing at 500 °C (~30 °C below the reverse martensite-to-austenite phase transformation temperature [6]) caused the development of recovery and primary recrystallization (Fig. 1c). It is worth noting that the reverse martensite-to-austenite phase transformation within packet-like areas resulted in the formation of almost fully austenitic packets (Fig. 1c) that is believed to develop through the lath-to-lath martensitic (shear) mechanism as per Kurdjumov-Sachs orientation relationship and a high amount of dislocation within [9]. However, an almost completely globular structure was still observed nearby the surface (Fig. 1f). Besides, a few lath-like nuclei of the reversed austenite can also be found within α'-martensite grains (Fig. 1f). In addition, $Me_{23}C_6$-type carbide particles of ~ 12 nm in diameter were located at grain/subgrain boundaries (Fig. 1f) and many nanocarbides of ~ 6 nm size were found mostly within the α'-martensite grains (Fig. 1g and h) due to lower carbon solubility in comparison to austenite. After the annealing, the average size of grains/subgrains decreased from ~ 170 nm to ~ 110 nm in the center and from ~ 180 to ~ 170 nm at the edge.

Ferromagnetic α-phase with a volume fraction of ~ 2% was uniformly distributed along a diameter of the initial bar (Fig. 2a). After cold swaging, the content of the α-phase was 39% and 68% in the center and at the edge, respectively (Fig. 2a) due to a gradual decrease in strain from the edge to the center during swaging [4]. Annealing at 500 °C was associated with a minor decrease in the amount of the α-phase (~4%) caused by the reverse transformation [6].

A uniform distribution of hardness along the diameter was observed in the initial condition (Fig. 2b). After cold swaging, the hardness of both the center and edge increased to ~450HV. The increase in hardness is likely associated with a high volume fraction of α'-martensite at the edge that generated compressive and tensile residual stresses at the edge and in the center, respectively [10]. Meanwhile, the half-radius hardness was ~ 400HV, possibly due to the absence of stresses. After annealing, the hardness after annealing dramatically increased that might be associated with the precipitation of carbides in α'-martensite (Fig. 1g and h). Due to a higher content of α'-martensite, more significant hardening was detected at the edge (Fig. 2b).

The initial condition exhibited ordinary tensile behavior (Fig. 2c) and mechanical properties (Table 1) due to the uniform coarse-grained structure. Cold swaging resulted in the stress peak at low engineering strain (~1%) and a considerable increase in the strength characteristics (YS = 1405 MPa; UTS = 1410 MPa) and a decrease in ductility (δ = 11.2%). After annealing at 500 °C, a similar tensile behavior was observed, yet an additional increase in both YS and UTS to 1490 and 1550 MPa, respectively, were detected. Meanwhile, a negligible decrease in the total elongation was also obtained. The major strengthening (Table 1) after annealing at 500 °C might be ascribed to the carbide precipitation within α'-martensite (Fig. 1g and h). The evaluation of Orowan strengthening (Supplementary materials) revealed that an increase in strength to ~120 MPa at the center and ~240 MPa at the edge was expected due to different content of strengthened α′-martensite – ~34% and ~ 67%, respectively (Fig. 2a).

During the Charpy impact test, all the energy was consumed for the crack propagation only, due to the presence of fatigue cracks in all specimens (Fig. 3a–c). After cold swaging notch toughness dropped from 1.58 to 0.70 MJ/m^2 (Table 1), most likely due to the microstructure refinement [11]. In comparison to the initial condition (Fig. 3a and d), the ratio of the plane strain zone and total fracture surface in the swaged condition increased from 0.36 to 0.53; this increase can be ascribed to a decrease in the energy consumption despite secondary cracking (Fig. 3b) and dimple failure structure (Fig. 3e). Unexpectedly, the annealing resulted in a doubling of the notch toughness level to 1.42 MJ/m^2. This increase was accompanied by a significant decrease in the area fraction of the plane strain zone to 0.11 (Fig. 3c) in spite of a dimple structure (Fig. 3f). On the other hand, carbide particles along grain/subgrain boundaries trigged most likely crack branching in the bar axis direction (Fig. 3g) thereby significantly increasing a path of crack growth and energy consumption.

4. Conclusions

In summary, the current study revealed the effect of cold swaging and subsequent annealing at 500 °C on the structure and mechanical properties of the AISI 321-type metastable austenitic stainless steel. Cold swaging to 90% of strain resulted in a noticeable variation in morphology and phase composition from the center to edge. After annealing at 500 °C, microstructure refinement due to the onset of recrystallization and reverse martensite-to-austenite transformation was detected. A significant strengthening was observed after annealing.

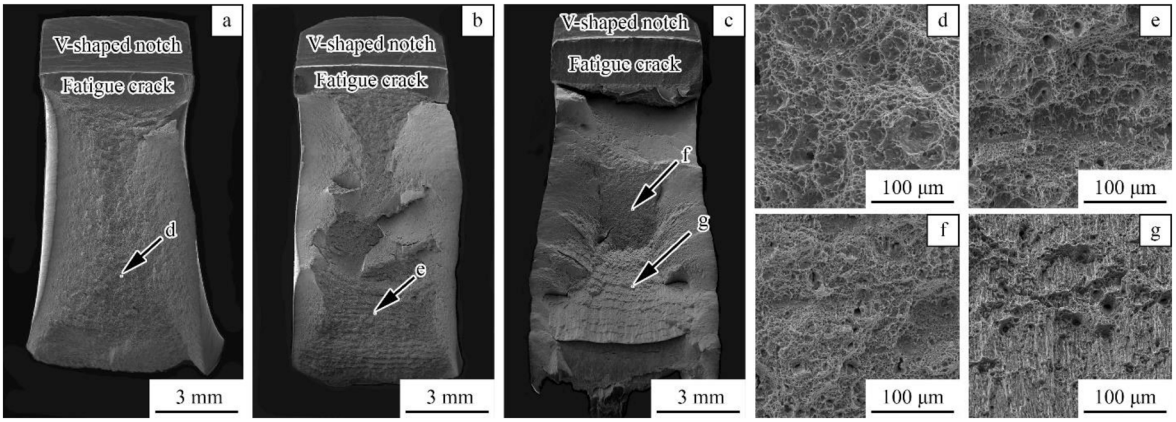

Fig. 3. (a)–(c) SEM-overviews of fracture surfaces and (d)–(g) SEM-micrographs of the fracture surfaces of the program steel in: (a), (d) – initial condition; (b), (e) – swaged condition, (c), (f), (g) – after annealing at 500 °C.

Meanwhile, notch toughness of the annealed condition almost reached the level of the initial condition.

CRediT authorship contribution statement

D.O. Panov: Investigation, Methodology, Visualization, Conceptualization, Writing - original draft. **R.S. Chernichenko:** Methodology, Visualization, Validation. **S.V. Naumov:** Methodology, Visualization, Validation. **A.S. Pertcev:** Methodology, Visualization, Validation. **N.D. Stepanov:** Writing - review & editing. **S.V. Zherebtsov:** Writing - review & editing. **G.A. Salishchev:** Writing - review & editing.

Declaration of Competing Interest

The authors declare that they have no known competing financial interests or personal relationships that could have appeared to influence the work reported in this paper.

Acknowledgments

This research was funded by the Russian Science Foundation Grant no. 20-79-10094. The authors are grateful to the personnel of the Joint Research Center, "Technology and Materials", Belgorod National Research University, for their assistance.

Appendix A. Supplementary data

Supplementary data to this article can be found online at https://doi.org/10.1016/j.matlet.2021.130585.

References

[1] K.H. Lo, C.H. Shek, J.K.L. Lai, Recent developments in stainless steels, Mater. Sci. Eng. R Rep. 65 (4-6) (2009) 39–104, https://doi.org/10.1016/j.mser.2009.03.001.
[2] J. Gu, L. Zhang, S. Ni, M. Song, Effects of grain size on the microstructures and mechanical properties of 304 austenitic steel processed by torsional deformation, Micron 105 (2018) 93–97, https://doi.org/10.1016/j.micron.2017.12.003.
[3] X.L. Wu, M.X. Yang, F.P. Yuan, L. Chen, Y.T. Zhu, Combining gradient structure and TRIP effect to produce austenite stainless steel with high strength and ductility, Acta Mater. 112 (2016) 337–346, https://doi.org/10.1016/j.actamat.2016.04.045.
[4] J. Domblesky, M. Mohamdein, R. Drab, R. Shivpuri, FEM Simulation of Multiple Pass Radial Forging of Pyromet 718, (2012) 251–262. https://doi.org/10.7449/1994/superalloys_1994_251_262.
[5] C. Lei, X. Deng, X. Li, Z. Wang, Simultaneous enhancement of strength and ductility through coordination deformation and multi-stage transformation induced plasticity (TRIP) effect in heterogeneous metastable austenitic steel, Scr. Mater. 162 (2019) 421–425, https://doi.org/10.1016/j.scriptamat.2018.12.007.
[6] D. Panov, E. Kudryavtsev, R. Chernichenko, A. Smirnov, N. Stepanov, Y. Simonov, S. Zherebtsov, G. Salishchev, Mechanisms of the reverse martensite-to-austenite transformation in a metastable austenitic stainless steel, Metals (Basel) 11 (2021) 1–13, https://doi.org/10.3390/met11040599.
[7] X. Huang, N. Hansen, N. Tsuji, Hardening by annealing and softening by deformation in nanostructured metals, Science 312 (2006) 249–251, https://doi.org/10.1126/science.1124268.
[8] D. Panov, A. Pertsev, A. Smirnov, V. Khotinov, Y. Simonov, Metastable austenitic steel structure and mechanical properties evolution in the process of cold radial forging, Materials 12 (2019) 2058, https://doi.org/10.3390/ma12132058.
[9] I. Shakhova, V. Dudko, A. Belyakov, K. Tsuzaki, R. Kaibyshev, Effect of large strain cold rolling and subsequent annealing on microstructure and mechanical properties of an austenitic stainless steel, Mater. Sci. Eng. A 545 (2012) 176–186, https://doi.org/10.1016/j.msea.2012.02.101.
[10] M. Halilovič, S. Issa, M. Wallin, H. Hallberg, M. Ristinmaa, Prediction of the residual state in 304 austenitic steel after laser shock peening – Effects of plastic deformation and martensitic phase transformation, Int. J. Mech. Sci. 111–112 (2016) 24–34, https://doi.org/10.1016/j.ijmecsci.2016.03.022.
[11] J. Li, W. Qin, P. Peng, M. Chen, Q. Mao, W. Yue, J. Kang, D. Meng, D. She, X. Zhu, Y. Li, Effects of geometric dimension and grain size on impact properties of 316L stainless steel, Mater. Lett. 284 (2021) 128908, https://doi.org/10.1016/j.matlet.2020.128908.